Ultrasound for Data Transfers from Deep Implants

an Experimental Comparison Between Binary-Frequency-Shift-Keying and On-Off-Keying with Backscatter Modulation

Holzapfel, Lukas; Giagka, Vasiliki

DOI
10.1109/IUS51837.2023.10308264

Publication date
2023

Document Version
Final published version

Published in
Proceedings of the 2023 IEEE International Ultrasonics Symposium (IUS)

Ultrasound for Data Transfers from Deep Implants: an Experimental Comparison Between Binary-Frequency-Shift-Keying and On-Off-Keying with Backscatter Modulation

Lukas Holzapfel*, Vasiliki Giagka*†
*Department of System Integration and Interconnection Technologies, Fraunhofer IZM, Berlin, Germany
†Department of Microelectronics, Delft University of Technology, Delft, The Netherlands
lukas.holzapfel@izm.fraunhofer.de, v.giagka@tudelft.nl

2023 IEEE International Ultrasonics Symposium (IUS) | 979-8-3503-4645-9/23/$31.00 ©2023 IEEE | DOI: 10.1109/IUS51837.2023.10308264

***Abstract*—Implantable devices need to communicate information to the outside world. For deep-seated miniaturized implants ultrasound communication can be favourable. However, implants need to operate during movement, and the selected communication scheme should be assessed accordingly. In this work, we implemented a simple protocol to transfer data packets based on On-Off-Keying (OOK) and Frequency-Shift-Keying (FSK) by backscatter modulation in ultrasonic communication links for deep implants. We then used it to compare FSK vs OOK encoding regarding the bit error rate during continuous ultrasound power transfer, and while moving, in a water tank setup. Our experiment shows, that sub-millimeter movements can have severe effects on OOK communication, but not for FKS. Therefore, FSK can allow for backscatter communication from deep implants regardless of their position and involved movements. The protocol can also be adapted to other backscatter modulation schemes in the future.**

***Index Terms*—backscatter, communication, implant, modulation, movement, ultrasound, wireless**

I. Introduction

In the recent years ultrasound has been researched as an alternative power source for miniaturized implants [1]–[3]. Ultrasound power transfer is particularly attractive for deep-seated implants, as those envisioned in bioelectronic medicine applications [4]. Bioelectronic medicine interacts with the peripheral nervous system using miniaturized neural interfaces, which can monitor or stimulate neural activity. These devices often need to communicate information regarding, for instance, stimulation efficacy, elicited neural signals [5][6] or parameters that reveal the integrity of the implant's encapsulation [7], [8]. In such cases a parallel ultrasonic communication channel is a natural solution [9]–[11]. On-Off Keying (OOK) is the most commonly used modulation protocol, because of the ease of its hardware implementation [12]. The carrier signal has to be simply turned on or off, depending on the current bit value, as shown in Fig. 1 a).

To further simplify the implant's circuitry and minimize its size and power demands, backscatter modulation is used [13].

This work is part of the Moore4Medical project funded by the ECSEL Joint Undertaking under grant number H2020-ECSEL-2019-IA-876190.

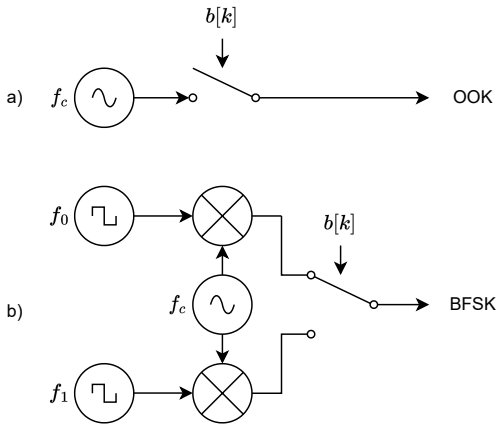

Fig. 1. Block diagrams comparing a) OOK and b) the proposed implementation for binary FSK. For OOK the sinusoidal carrier with frequency f_c is turned on or off depending on the current bit value $b[k]$. For FSK the carrier is multiplied by two square wave signals with frequencies f_0 and f_1. Depending on the current bit, one of the two modulated signals is selected.

For ultrasonic backscatter modulation, the implant modulates the electrical load connected to its power receiving transducer. Changing the electrical load, in turn, modulates the amount of reflected power, which can be detected by the external device. In its simplest form, load modulation is implemented by a single switch that briefly shorts the transducer. However, interference from other -possibly larger and closer- scatterers, like tissue-bone or tissue-gas interfaces, must be assumed to be present. The scattering from these reflectors cannot be assumed static and therefore the amplitude and phase of the interference must be assumed to change over time[12]. This makes the reception of ultrasonic backscatter signals based on amplitude modulation inherently difficult. We therefore proposed to combine backscatter modulation with two digital square wave modulation signals of different frequencies $f_{mod,0}$ and $f_{mod,1}$, to generate sidebands, thus effectively implementing binary Frequency-Shift Keying (FSK) [14], as shown in Fig. 1 b).

The following work describes a protocol to test the robustness of FSK against interference from other scattering compared to OOK and gives an overview of the results of those tests. To the best of our knowledge, movement has not been investigated in ultrasonic communication links so far.

II. Methods

The comparison of the modulation schemes was performed in a water tank setup, shown in Fig. 2 a). The following sections first give an overview of the experiment setup, and then discuss important aspects in more detail.

A. Transducer arrangement

For the experiment three transducers where placed in a water tank as shown in Fig. 2 b). As the external TX transducer, we used an unfocused commercial $1.27\,\mathrm{cm}$ submersible transducer with a resonant frequency of 5 MHz (V309-SU, Olympus). For the transducer at the implant side, we used one channel of a pre-charged capacitive micromachined ultrasound transducer (CMUT)-array, described in [15]. We placed the CMUT at a distance of approximately $11\,\mathrm{cm}$ on-axis of the externally driven transducer, because it gave us the maximum voltage across the CMUT. The CMUT was then connected to our prototyping platform. The backscattered ultrasound was picked up by a $1\,\mathrm{mm}$ diameter needle hydrophone (NH1000, Precision Acoustics) placed close to the TX transducer. During data transmission the CMUT was moved laterally out of the focal region at a speed of $\approx 18\,\mathrm{mm\,s^{-1}}$ to emulate a non-static environment.

B. Driving the external TX transducer

To emulate the external powering device, the external transducer was driven by a waveform generator (33622A, Keysight), set to a nominal output voltage of $10\,\mathrm{V_{pp}}$ with a $50\,\Omega$ load. The frequency was chosen to be close to the CMUT resonant frequency of $3.5\,\mathrm{MHz}$. As the reso nant frequency of the TX transducer is $5\,\mathrm{MHz}$, the efficiency of the transducer is decreased. However, since the focus of this work is not to maximize the power link efficiency, but to compare modulation schemes under the same conditions, this is not detrimental to the experimental results.

C. Modulating the backscattered ultrasound

The CMUT was connected to a prototyping platform we developed specifically for the evaluation of backscatter modulation schemes that can be implemented by a single load switch. Fig. 3 shows a block diagram of this platform. It is based on a STM32G474 microcontroller, and three Analog Devices ADG1401BRMZ analog switches. Each switch is controlled by one channel of the microcontroller's high resolution timer (HRTIM). For this experiment, however, only a single timer channel and analog switch was connected to the CMUT. The microcontroller is connected via USB to a PC for power supply and can be controlled using a text based protocol over a virtual COM port. Each of the three switching channels provides the possibility to populate an impedance

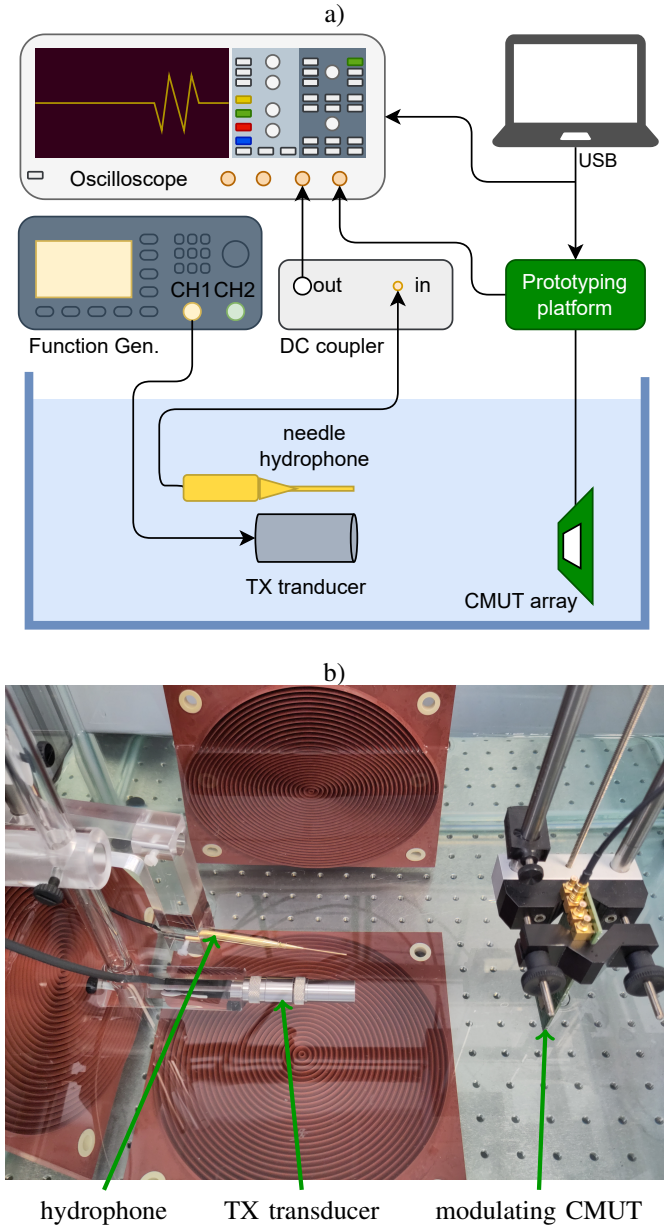

Fig. 2. The experimental setup used for the comparison of the two modulation schemes. a) Block diagram of the involved components. b) Arrangement of the transducers in the water tank.

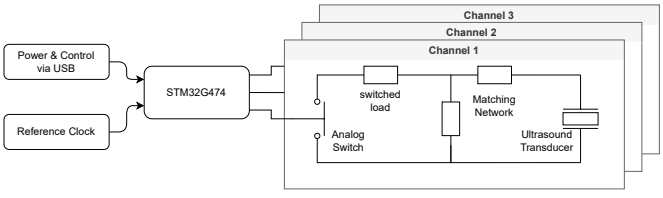

Fig. 3. Prototyping platform used to modulate the transducer load.

matching network and set the value of the switched load. For this experiment, the switched load was set to nominally $0\,\Omega$. After measuring the impedance of the CMUT in water, we adapted the impedance matching network accordingly. The experiment script, written in Python and running on the host PC, configures the prototyping platform to use OOK or FSK, and initiates the transfer of a packet of pseudo-random data. The packet starts with a 31-bit m-sequence preamble, followed by a payload, corresponding to a $1\,\mathrm{s}$ transfer duration. That is, for a symbol rate of $1\,\mathrm{kBd}$, the payload size was set to $1\,\mathrm{kbit}$. Approximately $200\,\mathrm{ms}$ after the transfer is initiated, the moving stage starts to move the CMUT.

D. Acquiring the backscattered signal

As the needle hydrophone has an internal preamplifier, it is powered by a DC coupler, which passes through the picked up AC signal to an oscilloscope (RTA4004, Rohde&Schwarz). The sample rate of the oscilloscope is set to $83.\bar{3}\,\mathrm{MHz}$ and the memory depth to 100 million samples. This equates to a duration of $1.2\,\mathrm{s}$ per acquisition. The oscilloscope is triggered by the prototyping platform, when the transfer is initiated. The signal is then transferred to a host PC, where it is processed using the receiver implementation described in section II-E.

E. Detection of the backscattered signal

The acquired signal is then processed immediately by the receiver shown in Fig. 4, which is implemented in Python, leveraging the Numpy and Numba packages, to achieve acceptable processing speeds. Due to the amount of data ($400\,\mathrm{MB}$ per

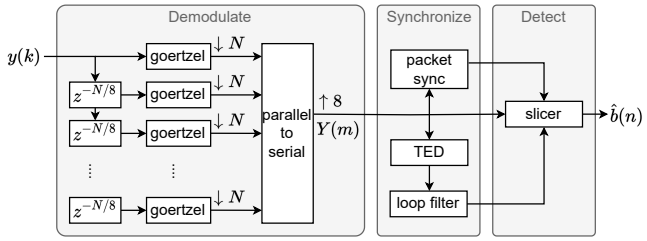

Fig. 4. Block diagram of the receiver implementation. The input signal $y(k)$ is demodulated in parallel for eight different phases, with a distance of $\frac{1}{8}$ of the Symbol length N between each phase. The parallel signals are then converted back into a single demodulated signal $Y(m)$. This signal is then used for packet and symbol time synchronization, and binary slicing, resulting in the estimated bit values $\hat{b}(n)$.

acquisition), we chose not to save the raw signal, but only the demodulated signal, loop filter output, and detected data. This way we can rerun the processing for all processing blocks working on the demodulated signal, which speeds up finding suitable parameter values for these processing blocks.

To demodulate the signal, we use the Goertzel algorithm, which we combine with windowing. In case of OOK, only the carrier frequency is demodulated. For FSK the first lower and upper modulation product for each of the two modulation frequencies -so in total four frequencies- are demodulated. To get a bipolar signal, the sum of the two modulation products for a binary 0, $Y_0(m) = Y(f_{0,l}, m) + Y(f_{0,u}, m)$, are subtracted from the sum of the two products of a binary 1, $Y_1(m) = Y(f_{1,l}, m) + Y(f_{1,u}, m)$:

$$Y(m) = Y_1(m) - Y_0(m) \tag{1}$$

We use eight parallel running demodulation filters with interleaved phases, to be able to synchronize further processing to the symbol timing later. The rate of the demodulated signal $Y(m)$ therefore is $\frac{8}{N}$ the rate of the incoming signal $y(k)$, with N being the number of samples acquired per symbol. The demodulated signal is fed into a Gardner timing error detector (TED), a preamble detector, and a slicer. The TED output is fed into a proportional-integral (PI) loop filter, which tells the slicer which sample to use for the next decision. Finding the packet start is based on the correlation of the signal to the preamble. Only if a packet preamble is detected, the output of the slicer is saved.

III. Results

Fig. 5 compares a demodulated bipolar signal for OOK and FSK. Both transfers, were performed for the same conditions

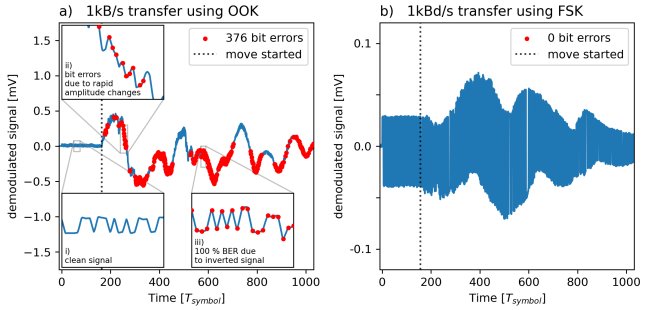

Fig. 5. Comparison of backscatter communication during movement using a) OOK and b) binary FSK. Amplitude and phase changes of the interference cause bit errors for OOK (insets ii and iii, respectively), while no bit errors occur for the same scenario using FSK. The amplitude changes of the interference are much higher than the amplitude of the useful signal for OOK. Note, that the offset at the beginning of the signal has been subtracted, which is why negative amplitudes seem to occur also for OOK.

involving movement. Fig. 5 a) shows the result for an OOK transfer. Before the movement starts, the modulation scheme performs well and no bit errors occur, as highlighted with inset i). However, during movement, rapid amplitude changes make it difficult for the slicer to adapt the decision boundary. Also, the phase difference between the interference and the useful signal cause intermittent cancellation and inversion of the useful signal. Both of these issues cause a high bit error rate for the OOK transfer.

Fig. 5 b) shows the result for an FSK transfer. The signal shows amplitude changes over time due to fading. However, these are not critical for the detection and no bit errors occur.

IV. Discussion

The results clearly show the advantages of FSK over OOK for backscatter communication. A communication link through tissue (phantoms) would have accounted for attenuation and more complex scattering. But, the underlying issues of

amplitude-based modulation can be sufficiently demonstrated in a motorized water tank setup. Further experiments are needed to compare these and other schemes, like Phase-Shift Keying by load modulation. Also transfers for different scenarios, for example with different positions, velocities and data rates.

V. Conclusion

Ultrasonic backscatter communication of deep implants suffers from non-static interference by other scatterers. We implemented a platform to benchmark backscatter communication schemes involving non-static interference and used it to compare FSK and OOK. The results show that amplitude-based modulation schemes, like OOK, can have high bit error rates due to the interference.

References

[1] F. Mazzilli, C. Lafon, and C. Dehollain, "A 10.5 cm ultrasound link for deep implanted medical devices," *IEEE Transactions on Biomedical Circuits and Systems*, vol. 8, no. 5, pp. 738–750, Oct. 2014, ISSN: 1940-9990. DOI: 10.1109/TBCAS.2013.2295403.

[2] L. Tacchetti, W. A. Serdijn, and V. Giagka, "An ultrasonically powered and controlled ultra-high-frequency biphasic electrical neurostimulator," in *2018 IEEE Biomedical Circuits and Systems Conference (BioCAS)*, Oct. 2018, pp. 1–4. DOI: 10.1109/BIOCAS.2018.8584718.

[3] Z. Kashani and M. Kiani, "A study on ultrasonic wireless power transfer with phased array for biomedical implants," *IEEE Transactions on Biomedical Circuits and Systems*, pp. 1–11, 2023, ISSN: 1940-9990. DOI: 10.1109/TBCAS.2023.3282197.

[4] V. Giagka and W. A. Serdijn, "Realizing flexible bioelectronic medicines for accessing the peripheral nerves – technology considerations," *Bioelectronic Medicine*, vol. 4, no. 1, p. 8, Jun. 26, 2018, ISSN: 2332-8886. DOI: 10.1186/s42234-018-0010-y. [Online]. Available: https://doi.org/10.1186/s42234-018-0010-y (visited on 08/05/2022).

[5] R. R. Harrison, "The Design of Integrated Circuits to Observe Brain Activity," *Proceedings of the IEEE*, vol. 96, no. 7, pp. 1203–1216, 2008, ISSN: 15582256. DOI: 10.1109/JPROC.2008.922581.

[6] Y. Liu, A. Urso, R. M. Da Ponte, *et al.*, "Bidirectional bioelectronic interfaces: System design and circuit implications," *IEEE Solid-State Circuits Magazine*, vol. 12, no. 2, pp. 30–46, 2020. DOI: 10.1109/MSSC.2020.2987506.

[7] C. O. Akgun, K. Nanbakhsh, V. Giagka, and W. A. Serdijn, "A chip integrity monitor for evaluating moisture/ion ingress in mm-sized single-chip implants," *IEEE Transaction Biomed. Circuits Syst.*, vol. 14, no. 4, pp. 658–670, Aug. 2020. DOI: 10.1109/TBCAS.2020.3007484.

[8] G. Rodrigues, M. Neca, J. Silva, *et al.*, "Towards a wireless system that can monitor the encapsulation of mm-sized active implants in vivo for bioelectronic medicine," in *2021 IEEE Conference on Neural Engineering (NER)*, May 2021, pp. 1–4. DOI: 10.1109/NER49283.2021.9441398.

[9] M. M. Ghanbari, D. K. Piech, K. Shen, *et al.*, "A sub-mm 3 ultrasonic free-floating implant for multi-mote neural recording," *IEEE Journal of Solid-State Circuits*, vol. 54, no. 11, pp. 3017–3030, 2019. DOI: 10.1109/JSSC.2019.2936303.

[10] M. J. Weber, Y. Yoshihara, A. Sawaby, *et al.*, "A high-precision 36 mm3 programmable implantable pressure sensor with fully ultrasonic power-up and data link," in *2017 Symposium on VLSI Circuits*, Jun. 2017, pp. C104–C105. DOI: 10.23919/VLSIC.2017.8008564.

[11] S. Kawasaki, I. Subramaniam, M. Saccher, and R. Dekker, "A microwatt telemetry protocol for targeting deep implants," in *2021 IEEE International Ultrasonics Symposium (IUS)*, IEEE, 2021, pp. 1–4. DOI: 10.1109/IUS52206.2021.9593603.

[12] B. Jaafar, J. Neasham, and P. Degenaar, "What ultrasound can and cannot do in implantable medical device communications," *IEEE Reviews in Biomedical Engineering*, vol. 16, pp. 357–370, 2023, ISSN: 1941-1189. DOI: 10.1109/RBME.2021.3080087.

[13] M. M. Ghanbari and R. Muller, "Optimizing volumetric efficiency and backscatter communication in biosensing ultrasonic implants," *IEEE Transactions on Biomedical Circuits and Systems*, vol. 14, no. 6, pp. 1381–1392, Dec. 2020, ISSN: 1940-9990. DOI: 10.1109/TBCAS.2020.3033488.

[14] L. Holzapfel and V. Giagka, "A robust backscatter modulation scheme for uninterrupted ultrasonic powering and back-communication of deep implants," biorxiv, preprint, Aug. 25, 2022. DOI: 10.1101/2022.08.23.503752. (visited on 07/28/2023).

[15] S. Kawasaki, Y. Westhoek, I. Subramaniam, M. Saccher, and R. Dekker, "Pre-charged collapse-mode capacitive micromachined ultrasonic transducer (CMUT) for broadband ultrasound power transfer," in *2021 IEEE Wireless Power Transfer Conference (WPTC)*, Jun. 2021, pp. 1–4. DOI: 10.1109/WPTC51349.2021.9458104.